Nanoscale-Confined and Fractional Crystallization of Poly(ethylene oxide) in the Interlamellar Region of Poly(butylene succinate)

Yong He, Bo Zhu, Weihua Kai, and Yoshio Inoue*

Department of Biomolecular Engineering, Tokyo Institute of Technology, Nagatsuta 4259, Midori-ku, Yokohama 226-8501, Japan

Received December 12, 2003; Revised Manuscript Received February 20, 2004

ABSTRACT: The miscibility, morphology, and crystallization behavior of the blend of poly(ethylene oxide) (PEO) and poly(butylene succinate) (PBS) have been investigated using differential scanning calorimetry, high-resolution solid-state ^{13}C NMR spectroscopy, and wide- and small-angle X-ray diffraction. PEO and PBS are found to be miscible in the amorphous phase, and fractional crystallization of PEO component is observed in the blends with low PEO content. Also, it is revealed that the PEO component in the blend with less than 20 wt % PEO content is completely included in the region between PBS lamellae. On the basis of these results, the crystallization behavior of the PEO component has been analyzed and the origin of fractional crystallization has been explored. The blend system of PBS and PEO investigated here is the first instance of confined and fractional crystallization occurring in a miscible blend.

1. Introduction

The process of crystallization of polymers from the molten state can be divided into two stages, nucleation and crystal growth. The nucleation stage is the process where the crystalline nuclei are formed in the molten state. The nuclei can be formed homogeneously by means of statistical fluctuation in the molten phase, or heterogeneously when it is induced by the presence of heterogeneities.

Semicrystalline polymers in the molten state usually nucleate on existing heterogeneities (catalyst debris, impurities, and other types of heterogeneities of unknown nature). However, if a semicrystalline polymer is finely dispersed in an immiscible matrix as isolated domains whose number is significantly greater than the number of active heterogeneities, some of the domains are completely free from any active heterogeneity and the crystallization in these domains can only proceed via a homogeneous nucleation at the largest supercoolings. When such a dispersed system is cooled from the melt, very often a series of crystallization exotherms can be observed and a fractional crystallization phenomenon occurs. The fractional crystallization phenomenon has been interpreted as the crystallizations of a series of groups of domains at specific and independent supercoolings.[1] The different groups of domains contain different heterogeneities with differing efficiency to induce the nucleation or even do not contain any heterogeneity and thus they crystallize at different temperatures.[1]

The fractional crystallization phenomenon has been the subject of many investigations. This phenomenon occurs in droplet suspension[2] and in immiscible polymer blends, such as poly(vinylidene fluoride)/polyamide,[3−5] polyolefins/polystyrene (PS),[1,6,7] poly(ethylene terephthalate)/polycarbonate,[8] poly(methylene oxide)/PS/poly(2,6-dimethyl-1,4-phenylene ether),[9] and poly(ethylene oxide) (PEO)/isotactic polypropylene.[10] Frensch et al.[4] have reviewed the earlier literature on this subject, and Arnal et al.[1] have presented a short review of current related literature.

Recently, the confined and fractional crystallizations of block copolymers have also attracted much attention. Muller et al. have synthesized a series of microphase-separated block copolymers incorporating one or two of the crystallizable blocks and examined their crystallization behavior.[11−13] They found that a fractional crystallization process occurs when the crystallizable block is the minor phase. In some cases, they also observed exclusive crystallization from the homogeneous nuclei.

As reviewed above, the fractional crystallization occurs in an immiscible blend or a microphase-separated block copolymer. As far as we know, there are no reports so far addressing the fractional crystallization behavior for a miscible blend and giving a systematic analysis. This work will present the first instance that confined and fractional crystallization happens even in a miscible blend.

In the present paper, we address the crystallization behavior in a miscible blend of poly(ethylene oxide) (PEO) and poly(butylene succinate) (PBS); both components are crystalline polymers. The miscibility, morphology, and crystallization behavior of the blends are investigated using differential scanning calorimetry, high-resolution solid-state ^{13}C NMR spectroscopy, and wide- and small-angle X-ray diffraction. It is revealed that the PEO component in a blend with low PEO content is completely included in the region between PBS lamellae with the crystallization of PBS. Furthermore, it is suggested that this inclusion is the origin of the confined and fractional crystallization of the PEO component.

2. Experimental Section

2.1. Materials and Blend Preparation. Poly(ethylene oxide) (PEO) with a number-average molecular weight M_n of 2.0×10^4 was purchased from Nacalai Tesque Inc., Japan. Poly(butylene succinate) (PBS) ($M_n = 2.2 \times 10^4$; $M_w/M_n = 2.1$) was kindly supplied by Showa Highpolymer Co. Before use, PEO and PBS were purified by precipitation, respectively, into *n*-hexane and ethanol from chloroform solutions.

* To whom correspondence should be addressed. Telephone: +81-45-924-5794. Fax: +81-45-924-5827. E-mail: yinoue@bio.titech.ac.jp.

10.1021/ma035886g CCC: $27.50
Published on Web 04/01/2004

Blends of PBS and PEO were prepared by solution casting with chloroform as a common solvent. Both polymers were dissolved and mixed in chloroform with the desired mass proportions (total polymer concentration was 2 wt %), stirred well, and subsequently cast onto Teflon dishes. The solvent was allowed to evaporate for 24 h, and the resulting films were further dried under vacuum at room temperature for 1 week. The casting films were subsequently compression molded between two Teflon sheets with an appropriate spacer for 2 min at 150 °C under a pressure of 5 MPa, using a TOYOSEIKI laboratory press (MINI TEST PRESS-10), followed by fast cooling to room temperature between two iron plates. The blends are denoted as *x*/*y*, where *x* and *y* are the weight percentages of PBS and PEO, respectively.

2.2. Experimental Techniques. Differential scanning calorimetry (DSC) runs were mainly performed on a Perkin-Elmer Diamond DSC under ultrapure nitrogen with 5.5−6.0 mg samples encapsulated in aluminum DSC pans. Before the measurement, the calibration was always carried out with indium at the same scanning rate as employed in the measurements. A baseline was regularly checked using an empty sample pan. The areas and maximums of the crystallization exothermic peak and the melting endothermic peak were taken as the crystallization enthalpy and crystallization temperature (ΔH_c and T_c) and heat of fusion and melting temperature (ΔH_f and T_m), respectively. The mass crystallinity X_c was estimated from ΔH_f assuming the heats of fusion $\Delta H_f°$ of 100 wt % crystalline PBS and PEO are 102[14] and 208 J/g,[15−18] respectively.

The glass transition temperature T_g was determined by a SEIKO DSC 220 system. After the sample was held at 150 °C for 2 min, it was quenched to −100 °C using liquid nitrogen. Then it was heated at a rate of 20 °C/min to 150 °C and the DSC curve was recorded. T_g was taken as the value of the middle point of the transition.

The NMR experiments were performed at room temperature on a JEOL GSX-270 spectrometer operating at 67.9 MHz. Proton spin−lattice relaxation time in the laboratory frame (T_1^H) was determined by an inversion−recovery pulse (($\pi-\tau-\pi$)/2) followed by cross polarization to ^{13}C magnetization.[19] The spectra were measured at high-power proton dipolar decoupling (ca.47.1 kHz). Pulse repetition time was generally set at greater than $5T_1^H$, the magic angle spinning (MAS) rate was optimized at 5 kHz, and a $^1H-^{13}C$ cross-polarization (CP) time of 300 μs was taken. A total of 1024 transients were accumulated with 4K data points for each spectrum. ^{13}C NMR chemical shifts were referenced to the CH_3 resonance of hexamethylbenzene (HMB) as the external standard (17.4 ppm from TMS).

Wide-angle X-ray diffraction (WAXD) and small-angle X-ray scattering (SAXS) measurements were performed on a Rigaku RINT-2000 system (40 kV and 200 mA) at room temperature. Nickel-filtered Cu Kα radiation (λ = 0.154 nm) was used. WAXD patterns were recorded in the 2θ range of 5°−55° at a scan speed of 1.0°/min. SAXS profiles were recorded in the 2θ range of 0.1°−2.5°. Each step increased 2θ by 0.004°, and X-ray was collected for 20 s at each step.

3. Results

3.1. Thermal Analysis. The glass transition temperature (T_g) of PBS/PEO blends was plotted in Figure 1 as a function of blend composition. A single T_g was detected for each blend and its value increased with PBS weight content W_{PBS}, suggesting that PBS and PEO are miscible in the melt state over the entire composition range. This result is consistent with the work of Qiu et al.[20] They measured the glass transition temperature of the blend, calculated the interaction parameter, and concluded that PBS/PEO blends are thermodynamically miscible in the melt.[20]

The DSC cooling curves at a cooling rate of 10 °C/min (before the cooling, the sample was molten at 150 °C for 5 min to erase the thermal history) are summarized in Figure 2 for the PBS/PEO blends. In the temperature range shown in this figure, the exothermal peaks correspond to the crystallization of PEO component. For most of the blends, only one crystallization peak was observed. However, three crystallization peaks of PEO component were detected for the 70/30 (w/w) PBS/PEO blend, suggesting the occurrence of fractional crystallization. The value of the crystallization temperature (T_c), taken as the maximum of the crystallization peak (or the main crystallization peak when two or more peaks were observed), was plotted in Figure 3b against PEO weight content W_{PEO}. When W_{PEO} is high, T_c decreases slowly with the decrease of W_{PEO}. However, it drops quickly with the decrease of W_{PEO} at low W_{PEO} range. The crossover happens at W_{PEO} of about 40 wt %. As for the PBS component, its T_c is not very sensitive to composition, though a decreasing tendency with the

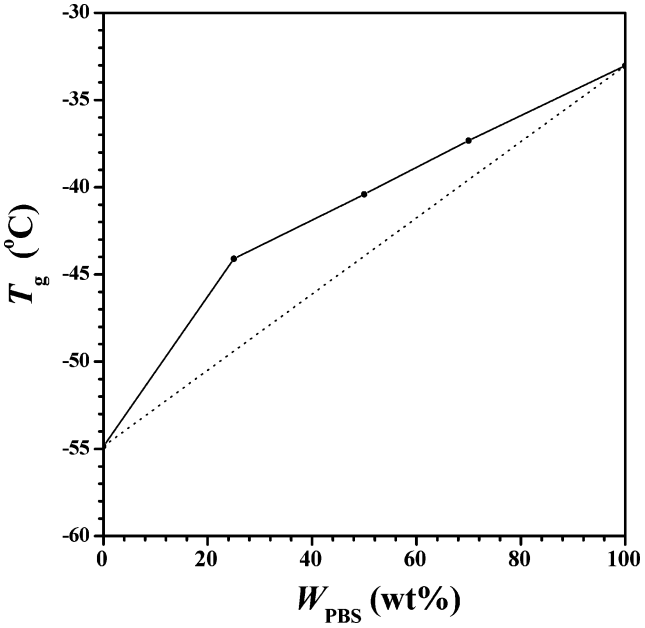

Figure 1. Glass transition temperatures, T_g's, of PBS/PEO blends as a function of PBS content, W_{PBS}.

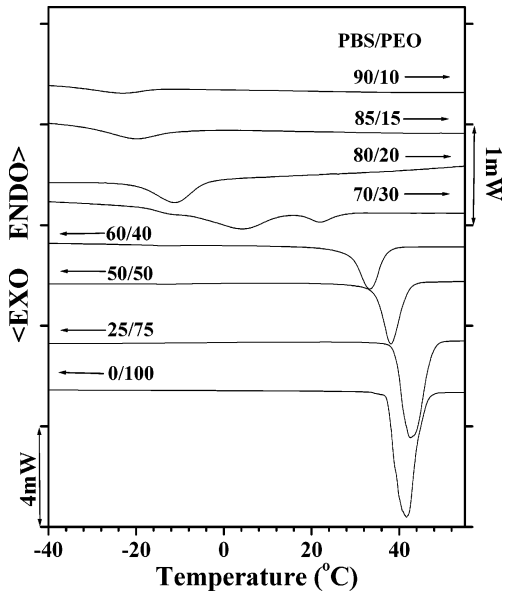

Figure 2. DSC cooling curves of PBS/PEO blends with PBS/PEO weight ratio 90/10 to 0/100. The cooling rate is 10 °C/min. Before cooling, the sample was molten at 150 °C for 5 min to erase the thermal history.

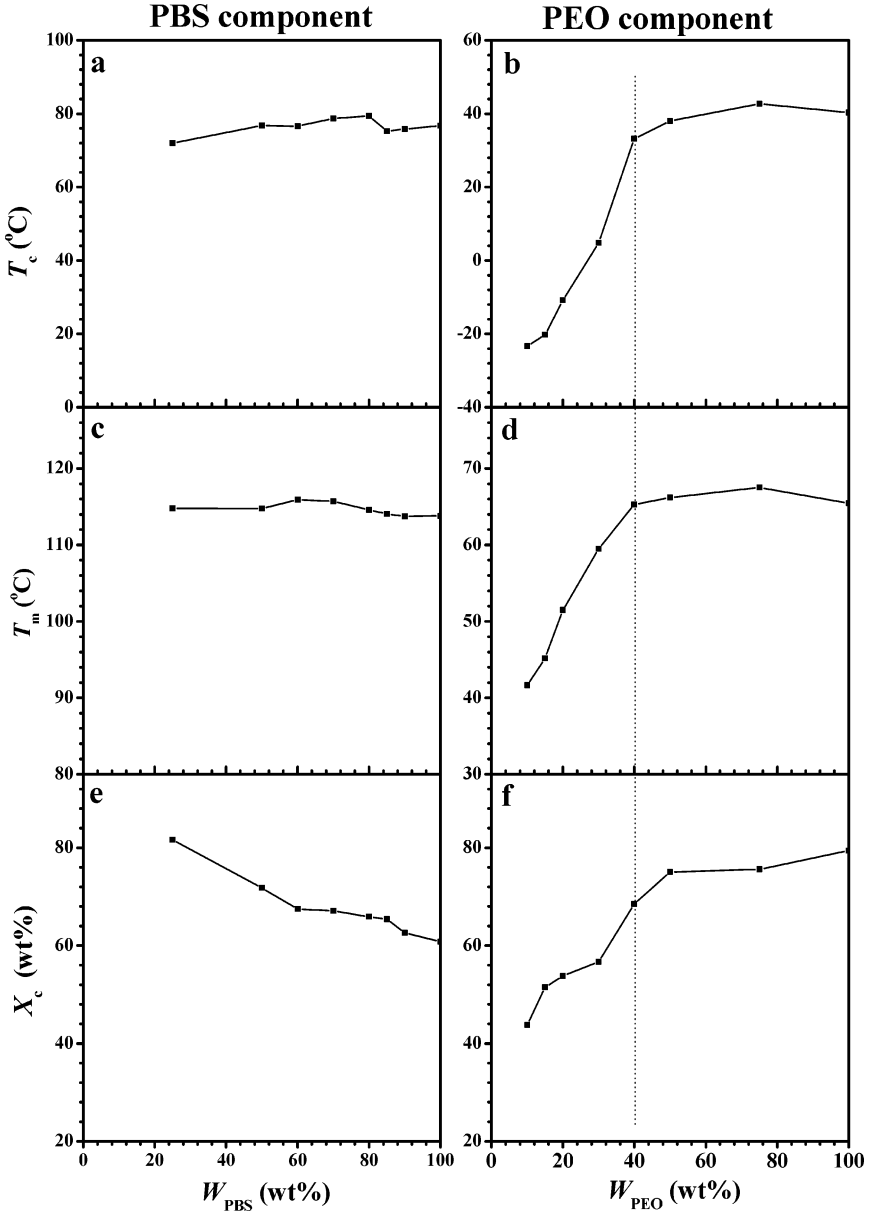

Figure 3. Crystallization temperatures, T_c's, melting temperatures, T_m's, and mass crystallinities, X_c's, of PBS component (a, c, and e) and PEO component (b, d, and f). The melting temperature and mass crystallinity were determined in subsequent heating scans (10 °C/min). In (b), T_c was taken as the maximum of the crystallization peak or the main crystallization peak when two or more peaks were observed.

decrease of PBS weight content, W_{PBS}, is observed (Figure 3a).

The melting temperatures (T_m's) recorded in the heating run (before the heating, the sample was molten at 150 °C for 5 min to erase the thermal history and then cooled to −50 °C at a scanning rate of 10 °C/min) are depicted in parts c and d of Figure 3 for the PBS and PEO components, respectively. Similar to the T_c, the T_m of the PBS component hardly changes while that of the PEO component varies obviously with the blend composition. Depending on the composition, the T_m of PEO component decreases slowly or quickly with decreasing W_{PEO}. In this case, the crossover also appears at W_{PEO} of about 40 wt %.

As for the mass crystallinity (X_c), that of the PBS component increases with the decrease of PBS content (Figure 3e), which may be a result of the decrease of T_g by blending with PEO. On the contrary, X_c of PEO decreases in the blend (Figure 3f). It drops at first slowly and then quickly with the decrease of W_{PEO}. Here, the crossover was also observed at a PEO content of about 40 wt %.

Here, it is noteworthy that the PEO component, in the blends with W_{PEO} less than 20 wt %, is completely free from the crystallization at room temperature under some conditions, as revealed by the DSC heating curves in Figure 4. When the blend was directly cooled from the molten state to room temperature and then aged at room temperature for 1 day before the DSC measurement, no endothermal peak corresponding to the melting of the PEO crystalline phase was detected (Figure 4, dotted lines), suggesting that the PEO component is completely prevented from the crystallization under this condition. In fact, it is found that the PEO component in these blends remains amorphous even if it is aged at room temperature for 1 week regardless of the cooling rate from the melt. However, the melting peak of the PEO component appears once the sample was quenched

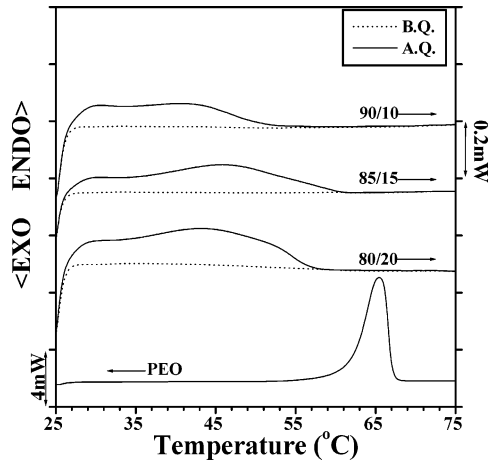

Figure 4. DSC heating curves (heating from 25 to 150 °C with a scanning rate of 10 °C/min) of molded blend films before and after they were quenched to liquid nitrogen. Thermal history of the molded films *before the quench*: compression molded at 150 °C for 2 min followed by a fast cooling to room temperature between two iron plates, then aging at room temperature for 1 day. *After the quench*, the films were further quenched to liquid nitrogen. "B.Q." and "A.Q." are the abbreviations of "before quench" and "after quench", respectively.

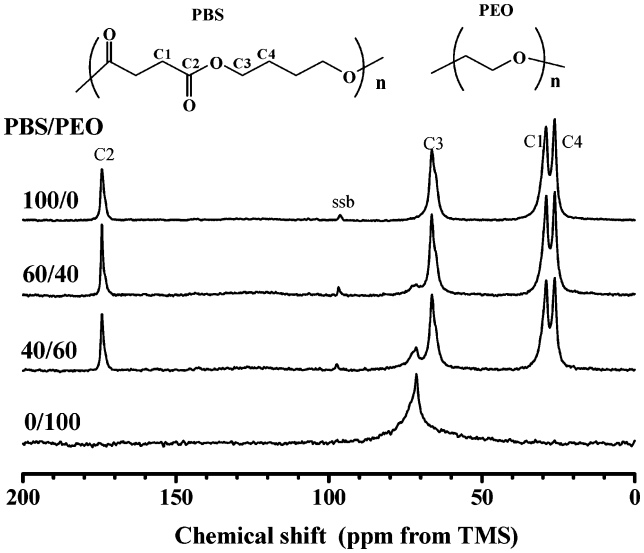

Figure 5. CP/MAS spectra and assignments of pure PBS (100/0), pure PEO (0/100), and their blends with PBS/PEO weight ratios of 60/40 and 40/60. "ssb" denotes the spinning sideband.

to liquid nitrogen (Figure 4, solid lines), which indicated that the PEO component in these blends could only crystallize at a temperature below room temperature. The WAXD patterns also provide the evidence supporting this conclusion (Figure 7), which will be referred to in section 3.3.

3.2. Solid-State ^{13}C NMR Spectroscopy. Cross-polarization (CP)/magic angle spinning (MAS) solid-state ^{13}C NMR spectroscopy has been established as a valuable tool for the study of the miscibility and microstructure of polymer blends on a molecular level. The proton spin−lattice relaxation times for the specific carbons in the blend permit an analysis and identification of the microheterogeneous phases.[21−23] The CP/MAS ^{13}C NMR spectra and the assignments of pure PBS, pure PEO, and their 40/60 and 60/40 (w/w) blends are given in Figure 5. Proton relaxation behavior in the laboratory frame is illustrated in Figure 6a, and the relaxation time (T_1^H) is plotted against the PBS content

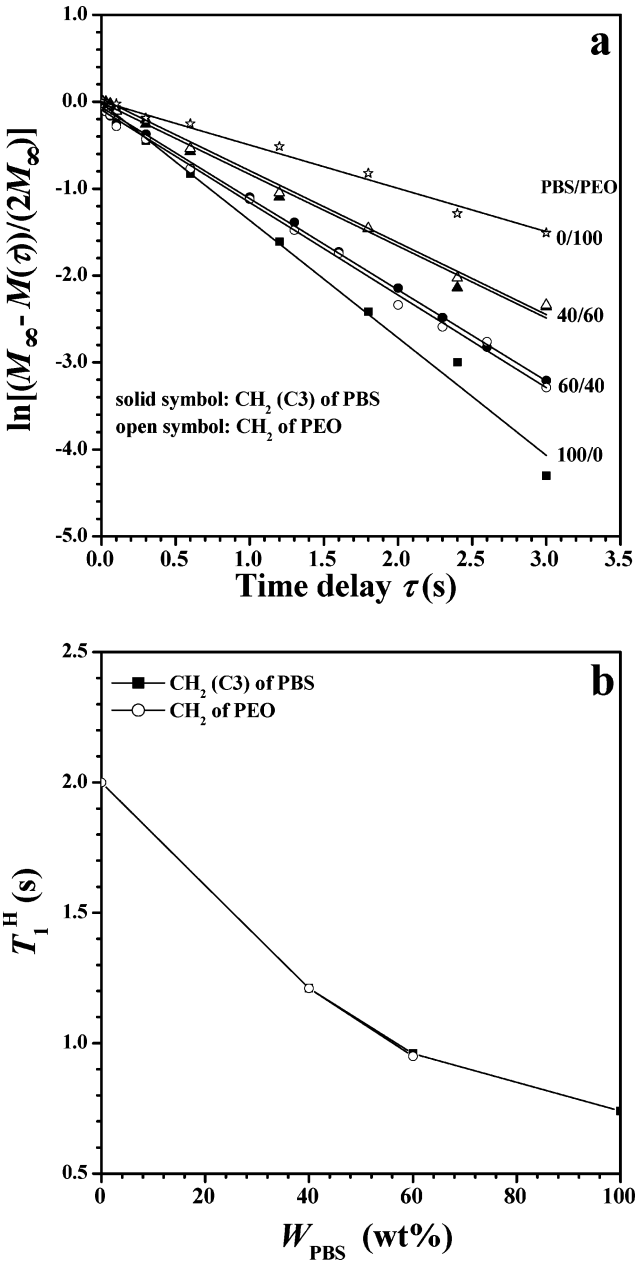

Figure 6. Proton spin−lattice relaxation behavior of pure PBS (100/0), pure PEO (0/100), and their blends with PBS/PEO weight ratios of 60/40 and 40/60. (a) Plots of $\ln[(M_\infty - M(\tau))/(2M_\infty)]$ against time delay τ. Here $M(\tau)$ and M_∞ represent the intensities of the carbon resonance at a given time delay τ and equilibrium state ($\tau > 5T_1^H$), respectively. (b) Proton spin−lattice relaxation time T_1^H as a function of blend composition.

in Figure 6b. All the relaxations were approximated by single-exponential processes even for the blends. The T_1^H values of pure PBS and pure PEO are 0.74 and 2.0 s, respectively, while those for the 60/40 and 40/60 (w/w) blends are averaged by spin diffusion to respectively 0.95 and 1.2 s. These results suggest that PBS and PEO are miscible on the observation scale of NMR T_1^H, which is in agreement with and confirms the conclusion derived from the DSC results.

3.3. X-ray Analysis. The WAXD patterns of pure PBS, pure PEO, and their blends measured at room temperature are shown in Figure 7. Obviously, the patterns of the blends are just the superimposition of those of pure PEO and PBS. Comparing the WAXD

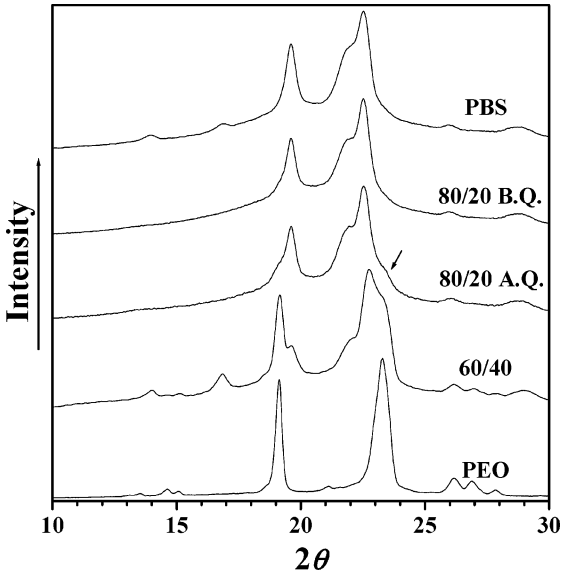

Figure 7. WAXD patterns of pure PBS (100/0), pure PEO (0/100), and their blends of 80/20 and 60/40. Before the measurement, the molded films of 100/0, 60/40, and 0/100 were aged at room temperature for at least 10 days. For the 80/20 film, see the caption of Figure 4 for the thermal history and the abbreviations.

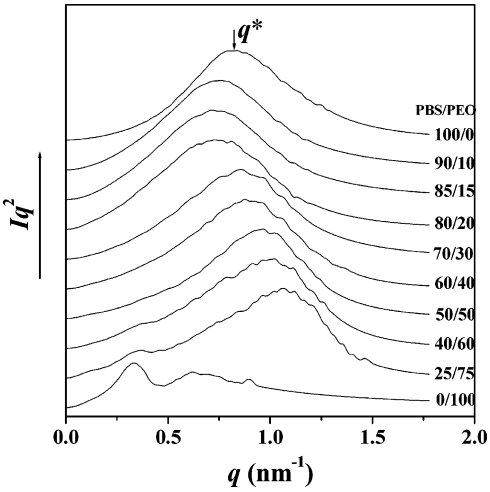

Figure 8. Lorentz-corrected SAXS profiles of molded blend films. The films used for SAXS measurements were aged at room temperature for 1 day after the mold. The quench to liquid nitrogen was not applied yet. The curves were normalized and shifted vertically for clarity.

patterns of the 80/20 (w/w) PBS/PEO blend before and after the quench, it is clear that the PEO component in this blend is in the amorphous state, as no peak corresponding to the diffraction of the PEO crystalline phase was detected when the blend was aged at room temperature after the melt. However, the crystallization of the PEO component immediately occurred once the blend was exposed to a thermal cycle passed through a temperature of about −10 °C or lower. This is consistent with the DSC results shown in Figure 4.

The microstructures of the PBS/PEO blends were probed by SAXS at room temperature. The Lorentz-corrected SAXS profiles of the PBS/PEO blends are summarized in Figure 8, where the scattering vector $q = 4\pi \sin \theta/\lambda$, with 2θ as the scattering angle. The position of the scattering peak from the blend shifts to a lower scattering angle with increasing PEO content, W_{PEO}, when W_{PEO} in the blend is low, as shown in Figure

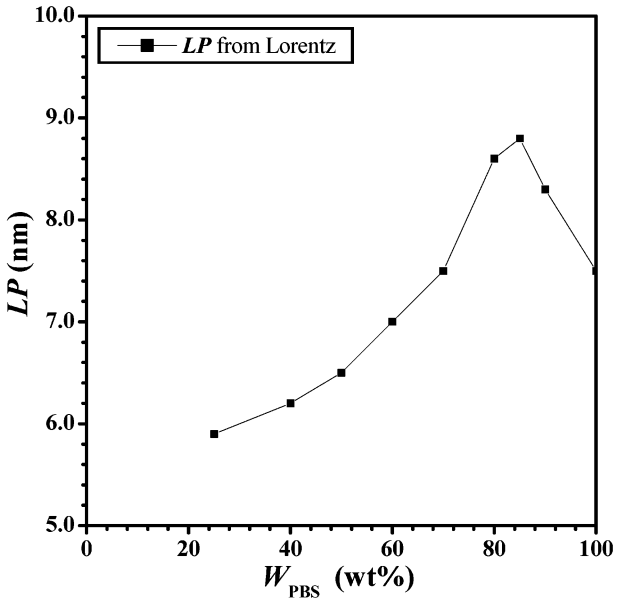

Figure 9. Relationship between the long period, LP, determined from Lorentz-corrected SAXS profiles (Figure 8) and blend composition.

8 for the 90/10 and 85/15 (w/w) PBS/PEO blends. However, the scattering peak again shifts to the high-q region with a further increase in W_{PEO}. A scattering shoulder begins to appear at the low-q range of the scattering peak when the W_{PEO} becomes greater than 50 wt %. The W_{PEO} dependence suggests that the scattering shoulder (or peak) should correspond to the scattering of the PEO component, as its position is almost the same as that of the PEO main scattering peak. Three peaks appear in the SAXS scattering profile of pure PEO, which were suggested to correspond to the first three orders of the crystalline repeat in the PEO spherulites.[24]

The long period or the interlamellar spacing of PBS in the blend was calculated from the equation $LP = 2\pi/q^*$, where q^* is the peak value found in the Lorentz-corrected SAXS plot (Figure 8). As shown in Figure 9, the long period of PBS in the blend at room temperature increases with increasing W_{PBS} up to 85 wt %. The maximum of the long period value of 8.8 nm was observed for the 85/15 (w/w) PBS/PEO blend. With further increase of the PBS content, W_{PBS}, the long period decreases rapidly and nearly linearly to 7.5 nm of pure PBS.

As suggested by the results from DSC and NMR relaxation measurements, PBS and PEO are miscible in the amorphous state. Also, the DSC and WAXD results have confirmed that the PEO component in the blends with PEO content no greater than 20 wt % is free from crystallization at room temperature after direct cooling from the melt. Thus, the 90/10 and 85/15 (w/w) PBS/PEO blends can be regarded as two-phase systems, that is, the PBS crystalline phase and the homogeneous amorphous phase composed of amorphous PBS and all PEO. Accordingly, the average thickness of the PBS crystalline phase and the average thickness of the amorphous phase of the blend as well as pure PBS homopolymer in the semicrystalline/amorphous state can be calculated from the normalized one-dimensional correlation function $\gamma(z)$.

The normalized one-dimensional correlation function $\gamma(z)$ was plotted in Figure 10 for pure PBS, 90/10 PBS/

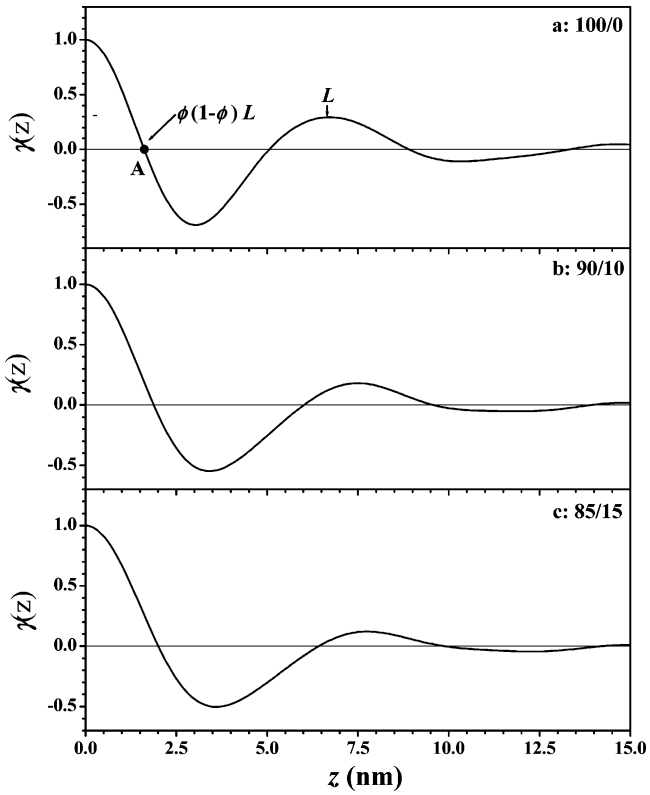

Figure 10. Normalized one-dimensional correlation functions $\gamma(z)$'s of PBS (100/0) and 90/10 and 85/15 (w/w) PBS/PEO blends.

PEO blend, and 85/15(w/w) PBS/PEO blend. As illustrated in Figure 10a, the long period L also can be estimated as the position of the first maximum of $\gamma(z)$. (In this study, two methods were used to estimate the long period. One is to get the long period from the Lorentz-corrected SAXS plot as shown in Figure 8, and the obtained long period is coded as LP. The other is to estimate it from $\gamma(z)$ as described here, and the resultant long period is expressed as L.) The linear crystallinity in the lamellar stacks ϕ can be calculated from the first intercept A of $\gamma(z)$ with the z-axis:[25,26]

$$A = \phi(1 - \phi)L \tag{1}$$

Note that eq 1 is quadratic in ϕ and can be solved to get two solutions for ϕ. As the mass crystallinity determined from DSC is greater than 50 wt % for pure PBS, 90/10 and 85/15 (w/w) PBS/PEO blends, the larger solution is taken as the appropriate solution. Employing a two-phase model, the average thickness of lamellar and amorphous layers (L_c and L_a) were evaluated from L and ϕ as:

$$L_c = \phi L \tag{2a}$$

$$L_a = L - L_c \tag{2b}$$

The obtained morphology parameters are listed in Table 1. Obviously, L, L_c, and L_a increase while the linear crystallinity in the lamellar stacks, ϕ, decreases after the inclusion of PEO.

The Lorentz-corrected SAXS profiles of 90/10, 85/15, and 80/20 (w/w) PBS/PEO blends before and after the quench are compared in Figure 11. The SAXS profile of pure PBS is also included in Figure 11 as a reference. As referred to above, the PEO component in these blends is free from crystallization before the quench while it is in the semicrystalline state after the quench. For the 90/10 and 85/15 (w/w) PBS/PEO blends, the peak position hardly changes with the quench; that is, LP does not change with the crystallization of PEO. However, the peak shows a tendency to shift to the high-q region for the 80/20 (w/w) PBS/PEO blend after the quench, implying that LP decreases after the crystallization of the PEO component.

The SAXS invariant Q_{exp} is determined from the SAXS intensity profile and depicted in Figure 12 for pure PBS and 90/10, 85/15, 80/20, and 70/30 (w/w) PBS/PEO blends. As the experimental invariant Q_{exp} is not on the absolute scale, in Figure 12 are given only the ratios of experimental invariants $Q_{exp,i}/Q_{exp,PBS}$ (experimental invariant of sample i/experimental invariant of pure PBS). $Q_{exp,i}/Q_{exp,PBS}$ is greater than 1 for all four blends, indicating that the addition of PEO to the blend increases the invariant in this composition range.

In the case that the PEO component is completely in the amorphous state and is entirely incorporated in the amorphous layers between PBS lamellae, the invariant Q_{int} of the ideal two phases can be calculated from the following equation:

$$Q_{int} = \phi(1 - \phi)(\eta_c - \eta_a)^2 \tag{3}$$

Here ϕ is the volume crystallinity. η_c and η_a are the electron densities of 100% crystalline PBS and the amorphous phase in the blend, respectively. η_a is determined by

$$\eta_a = (\eta_{a,PEO}\phi_{a,PEO} + \eta_{a,PBS}\phi_{a,PBS})/(\phi_{a,PEO} + \phi_{a,PBS}) \tag{4}$$

where $\phi_{a,PEO}$ and $\phi_{a,PBS}$ are the volume fractions of PEO and amorphous PBS in the blend, respectively. Electron densities of 100% crystalline PBS, 100% amorphous PBS, 100% crystalline PEO, and 100% amorphous PEO were calculated from their mass densities, namely, 0.716 ($\rho_{c,PBS} = 1.34$ g/cm^3, refs 27 and 28), 0.631 ($\rho_{a,PBS} = 1.18$ g/cm^3, refs 29 and 30), 0.676 ($\rho_{c,PEO} = 1.239$ g/cm^3, refs 31 and 32) and 0.612 ($\rho_{a,PEO} = 1.124$ g/cm^3, refs 31 and 32) mol of electrons/cm^3, respectively. ϕ, $\phi_{a,PEO}$, and $\phi_{a,PBS}$ can be estimated from the blend composition, mass crystallinity of PBS component, and the densities.

Figure 12 compares the ratio of experimental invariants ($Q_{exp,i}/Q_{exp,PBS}$, experimental invariant of sample i/experimental invariant of pure PBS) with the ratio of calculated ones ($Q_{int,i}/Q_{int,PBS}$). $Q_{exp,i}/Q_{exp,PBS}$ (the solid curve) agrees well with the corresponding $Q_{int,i}/Q_{int,PBS}$ (the dotted curve) for the 90/10, 85/15, and 80/20 (w/w) PBS/PEO blends, indicating that the PEO component is completely incorporated in the amorphous layers between the PBS lamellae in these blends.

4. Discussion

4.1. Miscibility of PBS/PEO Blend. Qiu et al. have reported that PBS and PEO are miscible in the molten state over the entire composition range.[20] In this work, two independent techniques, DSC and solid-state ^{13}C NMR, have been employed to evaluate the miscibility of the PBS/PEO blend. From DSC (Figure 1), a single and composition-dependent glass transition is observed over the whole composition range, suggesting that PBS and PEO are miscible in the amorphous phase. The results of solid-state ^{13}C NMR demonstrate that proton spin−lattice relaxations of the blends are completely

Table 1. Morphological Parameters of Pure PBS and 90/10 and 85/15 (w/w) PBS/PEO Blends at Room Temperature

sample	L/nm	L_a/nm	L_c/nm	ϕ	ϕ_b	ϕ_b/ϕ
PBS	6.6	2.8	3.8	0.58 ± 0.03	0.58 ± 0.02	1.00
90/10	7.6	3.5	4.1	0.54 ± 0.04	0.53 ± 0.02	0.98
85/15	7.9	3.7	4.2	0.53 ± 0.05	0.52 ± 0.02	0.98

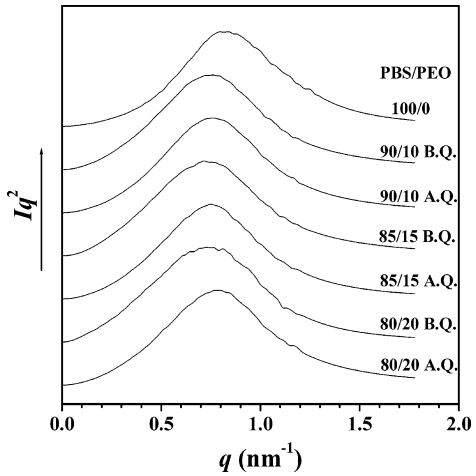

Figure 11. Lorentz-corrected SAXS profiles of 90/10, 85/15, and 80/20 (w/w) PBS/PEO blends before and after quench. The curves were normalized and shifted vertically for clarity. See the caption of Figure 4 for the thermal history of the sample and the abbreviations.

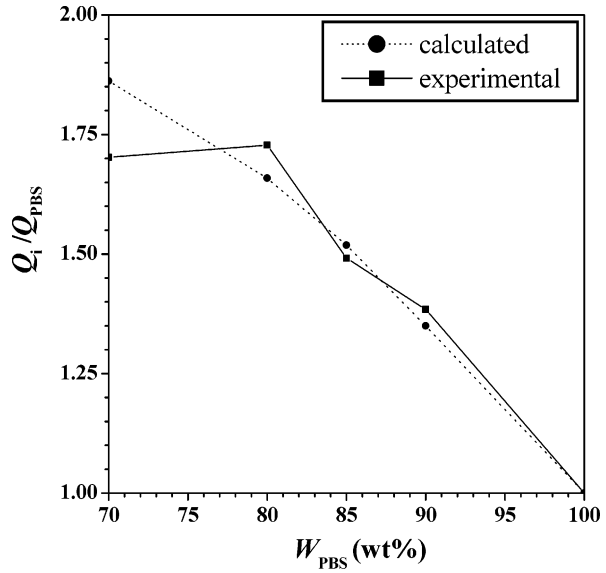

Figure 12. Ratios of invariant Q of samples to that of pure PBS.

averaged by spin diffusion (Figure 6), indicating the presence of a homogeneous mixture of PBS and PEO on the observation scale of T_1^H. In summary, both techniques give consistent results and umambiguously reveal that PBS and PEO are miscible in the amorphous phase.

4.2. Interlamellar Incorporation of PEO in the Blend with W_{PEO} < 20 wt % before the Crystallization of PEO. When W_{PEO} is less than 20 wt %, the long period, LP, increases with the increase of W_{PEO} (Figure 9), implying at least part of the PEO chains is included in the region between the PBS lamellae.

Comparing the linear crystallinity in the lamella stacks, ϕ, with the bulk volume crystallinity ϕ_b will clarify the distribution of amorphous PEO component. The bulk volume crystallinity, ϕ_b, of the blend can be estimated from the following equation before the crystallization of PEO component:

$$\phi_b = (W_{PBS}X_{c,PBS}/\rho_{c,PBS})/\{(W_{PBS}X_{c,PBS}/\rho_{c,PBS}) + [W_{PBS}(1 - X_{c,PBS})/\rho_{a,PBS}] + (1 - W_{PBS})/\rho_{a,PEO}\} \quad (5)$$

Here, W_{PBS} is the weight content of PBS. $X_{c,PBS}$ is the mass crystallinity of PBS component in the blend, which is determined from DSC. $\rho_{c,PBS}$, $\rho_{a,PBS}$, and $\rho_{a,PEO}$ are the densities of 100% crystalline PBS (1.34 g/cm^3, refs 27 and 28), 100% amorphous PBS (1.18 g/cm^3, refs 29 and 30), and 100% amorphous PEO (1.124 g/cm^3, refs 31 and 32), respectively.

Both ϕ and ϕ_b are listed in Table 1. Obviously, the value of ϕ is the same as that of ϕ_b within experimental uncertainty, indicating the complete incorporation of PEO component in the region between the PBS lamellae for the 90/10 and 85/15 (w/w) PBS/PEO blends.

Other evidence, which supports the complete interlamellar incorporation of PEO in the blends with W_{PEO} less than 20 wt %, comes from the invariant Q. As shown in Figure 12, $Q_{exp,i}/Q_{exp,PBS}$ agrees well with the corresponding $Q_{int,i}/Q_{int,PBS}$ for the 90/10, 85/15, and 80/20 (w/w) PBS/PEO blends, indicating that the PEO component is completely incorporated in the amorphous layers between the PBS lamellae in these blends. As for the 70/30 (w/w) PBS/PEO blend, the experimental one is somewhat lower than the calculated one, which may be due to (i) the crystallization of the PEO component and/or (ii) the diffusion of the PEO component from the interlamellar region. Both reduce the difference of electron density $\Delta\eta = \eta_c - \eta_a$ and lower $Q_{exp,i}/Q_{exp,PBS}$ for the 70/30 PBS/PEO blend.

Thus, the results from three aspects, which are the change of LP with composition (Figure 9), agreement between ϕ and ϕ_b (Table 1), and comparison between $Q_{exp,i}/Q_{exp,PBS}$ and $Q_{int,i}/Q_{int,PBS}$ (Figure 12), confirmed the complete incorporation of the PEO component into the region between the PBS lamellae in the blend with W_{PEO} less than 20 wt %.

As for the blends with high W_{PEO}, the distribution of PEO component is very complicated and only a brief discussion is given here, taking the 25/75 (w/w) PBS/PEO blend as an example. As the PEO component is no longer free from crystallization in this blend at room temperature, there are at least three phases: PEO crystalline phase, PBS crystalline phase, and homogeneous amorphous phase. Thus, it is difficult to get a reliable lamellar thickness from the normalized one-dimensional correlation function $\gamma(z)$, which is based on a two-phase model. However, it is reasonable to expect the lamellar thickness of PBS to be insensitive to or at least not to vary drastically with the blend composition, as the studied blend is a weakly interacting system. In fact, this assumption is supported by the fact that the melting point of the PBS component hardly changes with the composition of blend (Figure 3c). Thus, it is quite safe to say that the lamellar thickness of PBS in the 25/75 (w/w) PBS/PEO blend is comparable to that in pure PBS; that is, the lamellar thickness of PBS in the 25/75 (w/w) PBS/PEO blend should be close to 3.8 nm.

On the other hand, the lamellar thickness of PBS can be estimated from the following equation assuming a complete incorporation of PEO:

$$L_c = LP(W_{PBS}X_{c,PBS}/\rho_{c,PBS})/\{(W_{PBS}X_{c,PBS}/\rho_{c,PBS}) + [W_{PBS}(1 - X_{c,PBS})/\rho_{a,PBS}] + [(1 - W_{PBS})(1 - X_{c,PEO})/\rho_{a,PEO}] + (1 - W_{PBS})X_{c,PEO}/\rho_{c,PEO}\} \quad (6)$$

From this equation, L_c is estimated to be 1.1 nm for 25/75 blend. This conflicts with the above analysis, and the estimated value is almost the same as the fiber period of the unit cell (1.09 nm [28]), indicating that the hypothesis of complete incorporation is not right and a large part of the PEO component in the 25/75 (wt/wt) PBS/PEO blend is excluded from the interlamellar region to the interfibrillar or interspherulite region. The case should be similar for the other blends with $W_{PEO} \geq 50$ wt % as the long period LP of these blends is much lower than that of pure PBS (Figure 9).

4.3. Crystallization of PEO between the Lamellae of PBS. The results shown in the previous section revealed that the PEO component was completely incorporated into the region between PBS lamellae in the blends with $W_{PEO} < 20$ wt % before the crystallization of PEO. The next question is whether the PEO component remains in the interlamellar region after its crystallization. An indication for this question can be extracted from Figure 11, where the Lorentz-corrected SAXS profiles before the PEO crystallization are compared with those after the PEO crystallization. The peak position hardly changes with the quench; that is, LP does not change with the crystallization of PEO in the blend with $W_{PEO} < 20$ wt % (Figure 11). This fact implies that for the blend with $W_{PEO} < 20$ wt % the crystallization of the PEO component is confined in the amorphous layers (with an average thickness of about 3.5 nm, Table 1) between the PBS lamellae.

4.4. Nanoscale-Confined and Fractional Crystallization. So far, confined crystallizations have been well studied for block copolymers,[18,33−38] ultrathin films,[39−41] microdroplets,[2] and nanodroplets.[42] This work presents the first instance that confined crystallization of a blend component occurs in the region between the lamellae of another component. In block copolymer, the crystallizable block is confined within small isolated microdomains due to the microphase separation and often results in a fractional crystallization. In our case, the PEO component in the blend with $W_{PEO} < 20$ wt % is restrained in the interlamellar region of PBS with a thickness of about 3.5 nm as a result of the crystallization of the PBS component. With the crystallization of the PBS component in these blends, the amorphous phase (composed of amorphous PBS and all PEO) is divided into a large number of amorphous layers by the lamellae of PBS. These amorphous layers are isolated to some extent from each other. Thus, the crystallization of PEO in a layer is independent of that in another layer; that is, the crystallization in one layer is difficult to spread from this layer to another layer due to the confinement of the PBS lamellae. As the thickness of the amorphous layer is very small (about 3.5 nm), the number density of the amorphous layer is much higher than that of heterogeneities presented in the system. As a result, the fractional crystallization of PEO occurs or even exclusive crystallization induced by homogeneous nucleation is observed when the PEO content is low.

On the basis of the above analysis, it is now easy to understand the crystallization behavior of PEO in the blends. At high PEO content ($W_{PEO} \geq 40$ wt %), most of the PEO component is excluded from the interlamellar region and its crystallization is induced by active heterogeneous nucleation. The slow decrease of T_c with the decrease of PEO content should be mainly due to the weak interaction between PEO and PBS (Figures 2 and 3). At the middle PEO content ($W_{PEO} \sim 30$ wt %), the fraction of PEO in the interlamellar region of PBS is comparable to that beyond the interlamellar region. In this case, PEO beyond the interlamellar region of PBS crystallizes at low supercoolings by heterogeneous nucleation. However, the crystallization of PEO in the interlamellar region is mainly induced by less active heterogeneities at high supercoolings. As a result, fractional crystallization occurs (Figure 2). At low PEO content ($W_{PEO} \leq 20$ wt %), PEO component is completely included in the interlamellar region of PBS. The number of the amorphous layers is far bigger than that of available active heterogeneities. Under this condition, the crystallization of PEO component is basically induced by much less active heterogeneities or homogeneous nucleation at extreme supercoolings (Figures 2 and 3).

The melting behavior and the crystallinity of PEO can be also analyzed in a way similar to that for the crystallization behavior. The crossover of T_c, T_m, and X_c observed at a W_{PEO} of about 40 wt % is in essence just a reflection of the transformation from the inclusion of the PEO component in the interlamellar region of PBS at low PEO content to the exclusion of that at high PEO content.

Last, it is noteworthy that this confined and fractional crystallization also possibly occurs in other miscible binary blends of two crystalline polymers. Assuming that the two crystalline polymers are A and B, and A possesses lower T_c and lower T_m than B, the prerequisites for confined and fractional crystallization are the following: (i) A is divided by the lamellae, fibrils, and spherulites of B into micro- or nanodomains with the crystallization of B. These domains are free from each other to some extent. (ii) B does not induce the crystallization of component A. (iii) The number of the active heterogeneities in the blend is not too large. (iv) The T_g of B is not too high to completely prohibit the crystallization of A.

5. Conclusions

The miscibility, the morphology, and the crystallization behavior of PBS/PEO blends have been investigated using DSC, solid-state ^{13}C NMR, and wide- and small-angle X-ray diffraction. It was revealed that the PEO component is included in the interlamellar region of PBS and crystallizes between PBS lamellae when the PEO content in the blend is low. It is suggested that the inclusion of PEO component into the interlamellar region results in the confined and fractional crystallization. In essence, this confined and fractional crystallization is the same as what happens in block copolymers or immiscible blends.

References and Notes

(1) Arnal, M. L.; Matos, M. E.; Morales, R. A.; Santana, O. O.; Muller, A. J. *Macromol. Chem. Phys.* **1998**, *199*, 2275.
(2) Cormia, R. L.; Price, F. P.; Turnbull, D. *J. Chem. Phys.* **1962**, *37*, 1333

(3) Frensch, H.; Jungnickel, B. J. *Colloid Polym. Sci.* **1989**, *267*, 16.
(4) Frensch, H.; Harnischfeger, P.; Jungnickel, B. J. Fractional Crystallization in Incompatible Polymer Blends. In *Multiphase Polymers: Blends and Ionomers*; Utracky, L. A., Weiss, R. A., Eds.; ACS Symposium Series 395; American Chemical Society: Washington, DC, 1989; p 101.
(5) Frensch, H.; Jungnickel, B. J. *Plast. Rubber Compos. Process. Appl.* **1991**, *16*, 5.
(6) Arnal, M. L.; Müller, A. J.; Maiti, P.; Hikosaka, M. *Macromol. Chem. Phys.* **2000**, *201*, 2493.
(7) Arnal, M. L.; Müller, A. J. *Macromol. Chem. Phys.* **1999**, *200*, 2559.
(8) Molinuevo, C. H.; Mendez, G. A.; Muller, A. J. *J. Appl. Polym. Sci.* **1998**, *70*, 1725.
(9) Everaert, V.; Groeninckx, G.; Koch, M. H. J.; Reynaers, H. *Polymer* **2003**, *44*, 3491.
(10) Kowaleski, T.; Ragosta, G.; Martuscelli, E.; Galeski, A. *J. Appl. Polym. Sci.* **1997**, *66*, 2047.
(11) Muller, A. J.; Arnal, M. L.; Lopez-Carrasquero, F. *Macromol. Symp.* **2002**, *183*, 199.
(12) Arnal, M. L.; Balsamo, V.; Lopez-Carrasquero, F.; Contreras, J.; Carrillo, M.; Schmalz, H.; Abetz, V.; Laredo, E.; Mueller, A. J. *Macromolecules* **2001**, *34*, 7973.
(13) Mueller, A. J.; Balsamo, V.; Arnal, M. L.; Jakob, T.; Schmalz, H.; Abetz, V. *Macromolecules* **2002**, *35*, 3048.
(14) $\Delta H_f°$ of 100 wt % crystalline PBS was estimated by the following method: (a) Measure the mass of a dry volumetric flask (50 mL). (b) Add PBS pellets with a determined mass (∼20 g) and thermal history into the volumetric flask at 25 °C. (c) Fill the flask with distilled water to the mark and measure the total mass (PBS pellets + flask + water). (d) Calculate the density of PBS from the masses, the density of water, and the volume of flask. (e) Calculate the mass crystallinity of PBS with the published densities for 100% crystalline PBS (1.34 g/cm^3, refs 27 and 28) and 100% amorphous PBS (1.18 g/cm^3, refs 29 and 30). (f) Measure the heat of fusion of PBS using DSC. (g) Repeat steps a−f for PBS pellets with different thermal history. (h) Plot the heat of fusion against the mass crystallinity and a straight line is obtained. Extend the line to a mass crystallinity of 100 wt % to get $\Delta H_f°$.
(15) Campbell, C.; Viras, K.; Richardson, M. J.; Masters, A. J.; Booth, C. *Makromol. Chem.* **1993**, *194*, 799.
(16) Yang, Z.; Yu, G. E.; Cooke, J.; Ali-Adib, Z.; Viras, K.; Matsuura, H.; Ryan, A. J.; Booth, C. *J. Chem. Soc., Faraday Trans.* **1996**, *92*, 3173.
(17) Cooke, J.; Viras, K.; Yu, G. E.; Sun, T.; Yonemitsu, T.; Ryan, A. J.; Price, C.; Booth, C. *Macromolecules* **1998**, *31*, 3030.
(18) Xu, J.; Fairclough, J. P. A.; Mai, S.; Ryan, A. J.; Chaibundit, C. *Macromolecules* **2002**, *35*, 6937.
(19) Kwak, S.; Kim, J.; Kim, U. *Macromolecules* **1996**, *29*, 3560.
(20) Qiu, Z.; Ikehara, T.; Nishi, T. *Polymer* **2003**, *44*, 2799.
(21) McBrierty, V. J.; Douglass, D. C. *J. Polym. Sci., Macromol. Rev.* **1981**, *16*, 295.
(22) Linder, M.; Hendrichs, P. M.; Hewitt, J. M.; Massa, P. J. *J. Chem. Phys.* **1985**, *82*, 1585.
(23) Parmer, J. F.; Dickenson, L. C.; Chien, J. C. W.; Porter, R. S. *Macromolecules* **1989**, *22*, 1078.
(24) Dreezen, G.; Mischenko, N.; Koch, M. H. J.; Reynaers, H., Groeninckx, G. *Macromolecules* **1999**, *32*, 4015.
(25) Strobl, G. R.; Schneider, M. *J. Polym. Sci., Polym. Phys. Ed.* **1980**, *18*, 1343.
(26) Goderis, B.; Reynaers, H.; Koch, M. H. J.; Mathot, V. B. F. *J. Polym. Sci. B: Polym. Phys.* **1999**, *37*, 1715.
(27) Ihn, K. J.; Yoo, E. S.; Im, S. S. *Macromolecules* **1995**, *28*, 2460.
(28) Ichikawa, Y.; Kondo, H.; Igarashi, Y.; Noguchi, K.; Okuyama, K.; Washiyama, J. *Polymer* **2000**, *41*, 4719.
(29) Yoo, E. S.; Im, S. S. *J. Environ. Polym. Degrad.* **1997**, *7*, 19.
(30) Miyata, T.; Masuko, T. *Polymer* **1998**, *39*, 1399.
(31) Wunderlich, B. *Macromolecular Physics*; Academic Press: New York, 1980; Vol. 3, p 67.
(32) *Polymer Handbook*, 3rd ed.; Brandrup, J., Immergut, E. H., Eds.; Wiley: New York, 1989.
(33) Loo, Y. L.; Register, R. A.; Ryan, A. J. *Phys. Rev. Lett.* **2000**, *84*, 4120.
(34) Segalman, R. A.; Hexemer, A.; Kramer, E. J. *Macromolecules* **2003**, *36*, 6831.
(35) Schmalz, H.; Knoll, A.; Muller, A. J.; Abetz, V. *Macromolecules* **2002**, *35*, 10004.
(36) Schipper, F. J. M.; Floudas, G.; Pispas, S.; Hadjichristidis, N.; Pakula, T. *Macromolecules* **2002**, *35*, 8860.
(37) Opitz, R.; Lambreva, D. M.; de Jeu, W. H. *Macromolecules* **2002**, *35*, 6930.
(38) Zhu, L.; Huang, P.; Chen, W. Y.; Ge, Q.; Quirk, R. P.; Cheng, S. Z. D.; Thomas, E. L.; Lotz, B.; Hsiao, B. S.; Yeh, F.; Liu, L. *Macromolecules* **2002**, *35*, 3553.
(39) Schonherr, H.; Frank, C. W. *Macromolecules* **2003**, *36*, 1188.
(40) Schonherr, H.; Frank, C. W. *Macromolecules* **2003**, *36*, 1199.
(41) Reiter, G. *J. Polym. Sci., B: Polym. Phys.* **2003**, *41*, 1869.
(42) Taden, A.; Landfester, K. *Macromolecules* **2003**, *36*, 4037.

MA035886G